Supporting Information

Ameliorated trap density and energetic disorder by strengthened intermolecular interaction strategy to construct efficient non-halogenated organic solar cells

Shengzheng Gao[1], Yiming Zhang[2,3,4], Seonghun Jeong[5], Xinjie Zhou[1], Hao Xu[1], Shanlei Xu[1], Daqiang Chen[3,4], Wenzhu Liu[6], Changduk Yang[5,7*], Sheng Meng[3,4,8*], Weiguo Zhu[1], Xin Song[1,9*]

1: School of Materials Science and Engineering, Jiangsu Engineering Laboratory of Light-Electricity-Heat Energy-Converting Materials and Applications, Changzhou University, Changzhou 213164, P. R. China

2: School of Physics and Laboratory of Zhongyuan Light, Zhengzhou University, Zhengzhou 450001, P. R. China

3: Beijing National Laboratory for Condensed Matter Physics and Institute of Physics, Chinese Academy of Sciences, Beijing 100190, P. R. China

4: School of Physical Sciences, University of Chinese Academy of Sciences, Beijing 100049, P. R. China

5: School of Energy and Chemical Engineering, Perovtronics Research Center, Low Dimensional Carbon Materials Center, Ulsan National Institute of Science and Technology (UNIST), Ulsan 44919, South Korea;

6: Research Center for New Energy Technology, Shanghai Institute of Microsystem and Information Technology, Chinese Academy of Sciences, Shanghai 201800, China

7: Graduate School of Carbon Neutrality, Ulsan National Institute of Science and Technology (UNIST), Ulsan 44919, South Korea

8: Songshan Lake Materials Laboratory, Dongguan, Guangdong 523808, P. R. China

9: Key Laboratory of Advanced Energy Materials Chemistry (Ministry of Education), Nankai University, Tianjin 300071, P. R. China

Corresponding Author: xin.song@cczu.edu.cn, smeng@iphy.ac.cn, yang@unist.ac.kr

1. Materials

PM6 was purchased from Solarmer Materials Inc. 2PACz, BTP-eC9 was purchased from Dethon Optoelectronics Materials Inc. DBE was purchased from Sigma. PNDI-F3N-Br was purchased from FlexPV Optoelectronics Inc. All materials and solvents were commercially available and used as received.

2. Devices Fabrication

Photovoltaic devices

The devices were fabricated with conventional structures of ITO/HTL/BHJ/PDINN /Ag(100 nm). The patterned ITO glass substrates (SuZhou ShangYang Solar Technology Co., Ltd.) were cleaned sequentially under sonication with deionized water and isopropanol, and then dried at 60 ℃ in a baking oven overnight. After UV-ozone treatment for 15 min, a 2PACz layer (0.5 mg/ml) was spin-coated on ITO substrate at 3000 rpm for 30 s, and then baked in air at 100 ℃ for 5 min; Sequentially, the active layer solution of PM6:BTP-eC9 (1:1.2, toluene, 20 mg/ml) was spin-coated at 3000 rpm for 30 s without and with DBE additive. After that, PNDI-F3N-Br methanol solution with a concentration of 1.0 mg mL^{-1} (methanol) was spin-coated onto the active layer at 3000 rpm for 30 s. To complete the fabrication of the devices, 100 nm of Ag was thermally evaporated through a mask under a vacuum of ~5 × 10^{-4} mbar. The active area of the devices was 0.06 cm^2.

3. Devices characterization

J-V and EQE

The photovoltaic performance was measured under an AM 1.5G spectrum from a solar simulator (Newport). The current density-voltage (J-V) characteristics were recorded with a Keithley 2400 source meter. The light intensity of the light source was calibrated before the testing by using a standard silicon (Si) solar cell, as calibrated by a National Renewable Energy Laboratory (NREL) certified silicon photodiode, giving a value of 100 mW/cm^2. The external quantum efficiency (EQE) were obtained on a commercial EQE measurement system (Enlitech, QE-R3011). The light intensity at each wavelength was calibrated by a standard single-crystal Si photovoltaic cell. Highly sensitive EQE was conducted by an integrated system with Fourier transform photocurrent meter (PECT-600, Enlitech).

Density Functional Theory (DFT) Calculations

The structural optimization is performed via the Vienna *Ab initio* Simulation Package (VASP) 1 and the xTB[2] package at the GFN2-xTB level with BFGS algorithm. To obtain the ground state properties, using a projector-augmented wave (PAW) pseudopotential in conjunction with the Perdew–Burke–Ernzerhof (PBE) functional [2] and plane-wave basis set with energy cutoff at 400 eV. The atomic structure of systems are positioned in a cubic supercell of 42×42×42 Å^3 along three directions and fully relaxed until the force on each atom was less than 0.02 eV/Å. Monkhorst Pack k-point mesh of 1×1×1 was adopted for the calculations.

Space-Charge-Limited-Current (SCLC) Measurement

Hole-only and electron-only devices were fabricated to measure corresponding mobilities of active layers by using the space charge limited current (SCLC) method with structure of ITO/PEDOT:PSS/active layer/MoO$_3$/Ag and ITO/ZnO/active layer/ZnO/Ag, respectively. Here, the preparation of active layer was consistent with that of the photovoltaic devices. The mobilities (μ) were determined by fitting the dark current to the model of a single carrier SCLC, described by the equation:

$$J = \frac{9}{8} \varepsilon_0 \varepsilon_r \mu \frac{V^2}{d^3}$$

where J is the current, E is the effective electric field, ε_0 is the permittivity of free space, ε_r is the material relative permittivity, d is the thickness of the active layer, and V is the effective voltage. The effective voltage was obtained by subtracting the built-in voltage (V_{bi}, the built-in voltage due to the relative work function difference of the two electrodes) and the voltage drop (V_s, due to contact resistance and series resistance across the electrodes) from the applied voltage (V_{appl}), $V = V_{appl} - V_{bi} - V_s$ The mobility was calculated from the slope of the $J_{1/2}$-V curves. The thickness of the BHJ blend for SCLC measurement was about 90 nm.

Atomic Force Microscopy

Tapping-mode atomic force microscopy (AFM) images were obtained using a NanoScope NS3A system (Digital Instrument).

UV-vis Absorption Measurement

UV-vis absorption spectra were recorded on a Shimadzu spectrophotometer.

Transient Photocurrent and Photovoltage

In the TPC and TPV measurements, the OSCs were fabricated with the same method as mentioned above. The data were obtained by the all-in-one characterization platform, Paios (Fluxim AG, Switzerland).

FT-IR Characterization

FT-IR spectra were recorded on a PerkinElmer, Spectrum 100.

Deep level transient spectroscopy (DLTS) Test

The transient current response is analyzed by applying a negative voltage of -3V to the device in the dark. Using the following equation to estimate the defect distributions in organic semiconductors. Considering the dependence of carrier transport position in the device, the current peak in the first 0.1μs is mainly caused by the displacement current, so the fitting of 0.1 ~ 100μs at room temperature are dominant. The trapped defect state volume density Nt of the discrete energy trap can be expressed as:

$$j_{te}(t) = \frac{1}{\tau_{te}} \cdot q \cdot d \cdot N_t \cdot exp(-\frac{t}{\tau_{te}})$$

Where $j_{te}(t)$ is trap emission current, τ_{te} is catch-trap emission time constant, q is a single charge amount, d is the film thickness of the device, N_t is the trap state density.

GIWAXS Characterization

The GIWAXS data were collected at the DESY P03 beamline with an x-ray energy of 10.8 keV. The incidence angle was set to 0.12º and the sample-to-detector distance (210.98 mm) was calibrated with CeO_2 powder. The detector images were collected by the Lambda 7.5M detector and were reshaped using GIXSGUI package base-on MATLAB software.

Film-depth-dependent light absorption spectroscopy (FLAS)

The FLAS was performed by a homemade instrument by Lu et al[3,4]. A self-developed soft plasma source generated by glow-discharging of low-pressure oxygen was used to incrementally etch the film without degage to the underneath films, which were in-situ monitored by a spectrometer. The soft plasma source is employed to incrementally etch the film, without damage to the underneath materials. During the etching, the light absorption spectroscopy is in-situ measured. The main mechanism of FLAS is to divide the whole film into multiple sublayers with the absorbance spectrum of the whole film being equal to the sum of those of sublayers according to the Beer–Lambert law:

$$I = I_0 \prod_{i=1}^{n} 10^{-A_i} = I_0 10^{-\Sigma_i^n A_i} = I_0 10^{-A_{wf}}$$

$$A_{wf} = \sum_{i}^{n} A_i$$

where I_0 and I are intensity of light incident on the film and light passing through the film, respectively. A_{wf} and A_i are absorbance spectra of whole film and sublayer i, respectively. Therefore, the difference in absorbance spectrum before and after each etching (ΔA_{wf}) is considered as the spectrum of the sublayer (A_i) that has been etched away every single time.

The optical simulations of OSC devices often use the transporting matrix model, the extinction coefficient k is obtained through equation below.

$$A = -\lg\left(\exp\left(-\frac{4\pi\kappa d}{\lambda}\right)\right)$$

 where d is the thickness of each sublayer, λ is the wavelength, A is the absorbance, k is the extinction coefficient. As the calculated exciton generation rate is a function of position and wavelength, which reflects the generation rate of excitons when the active layer absorbs light with different wavelengths at different locations. Then after summarized the exciton generation in each sublayer with varied thickness, we can obtain the 2D exciton generation rate mapping contour.
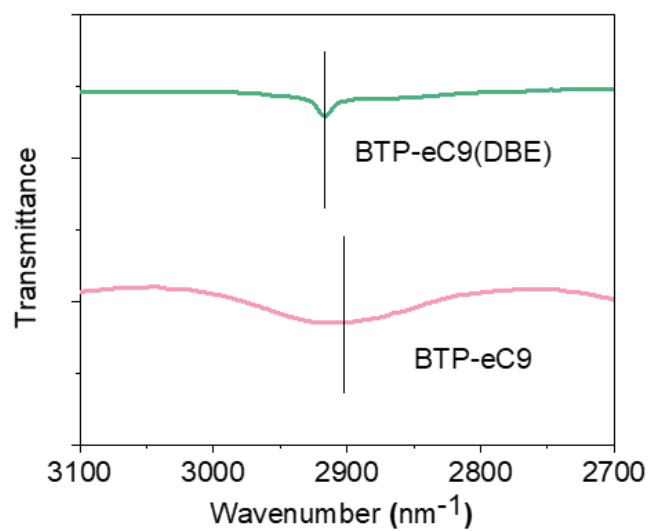
Figure S1. The FT-IR curves of BTP-eC9 film without and with DBE additive.
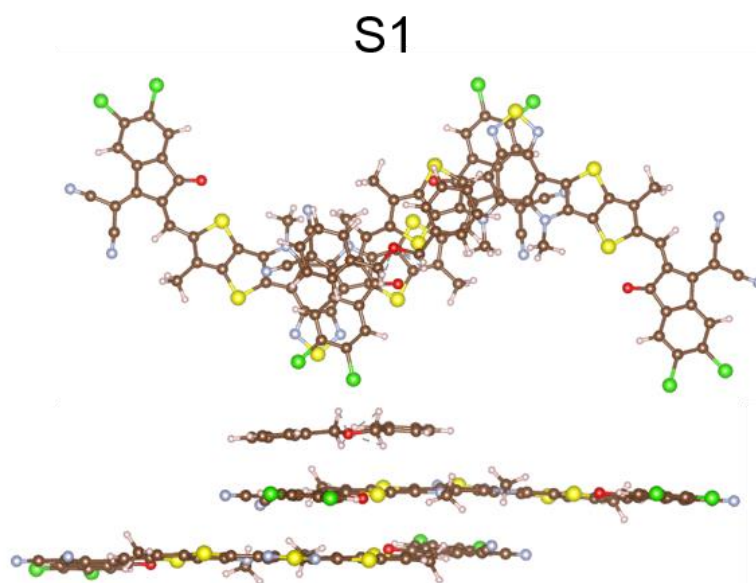
Figure S2. The planar and vertical feature of DBE adsorb on the BTP-eC9 dimer with S1 configuration. The calculated adsorption energy is -0.84 eV.
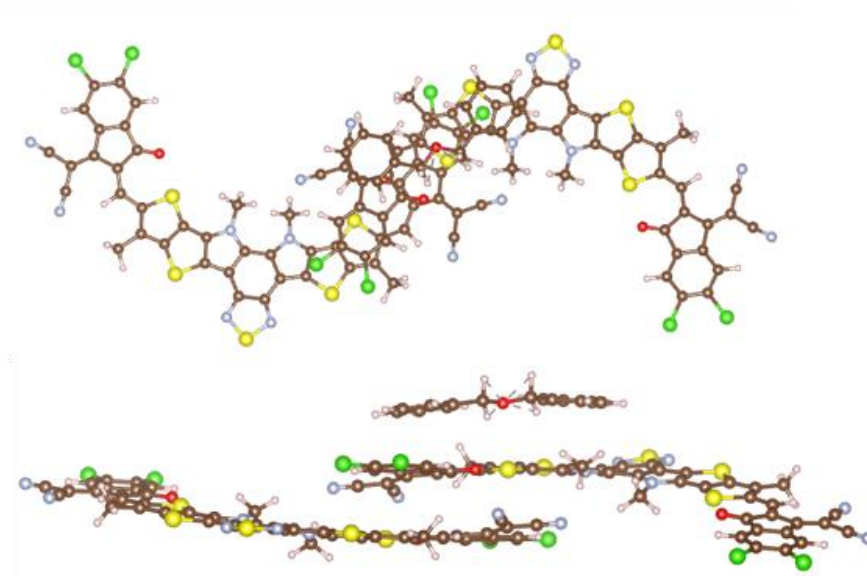
S2

Figure S3. The planar and vertical feature of DBE adsorb on the BTP-eC9 dimer with S2 configuration. The calculated adsorption energy is -0.86 eV.
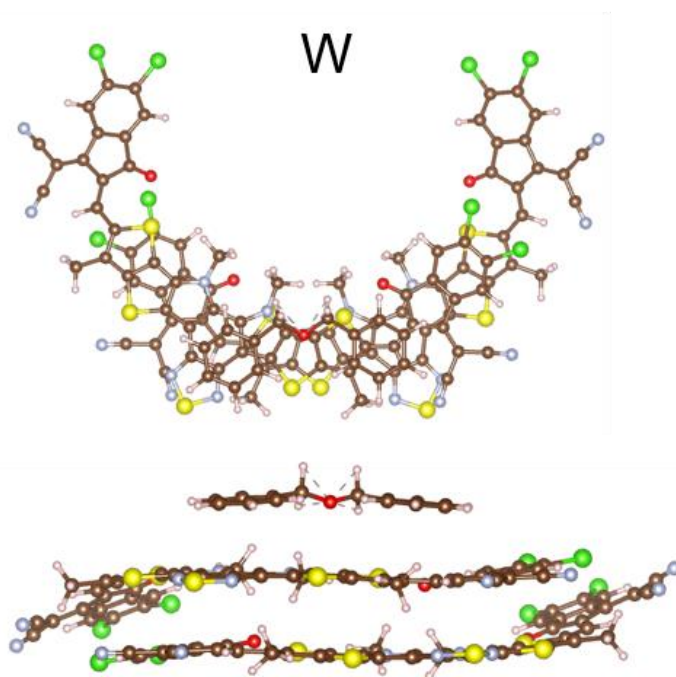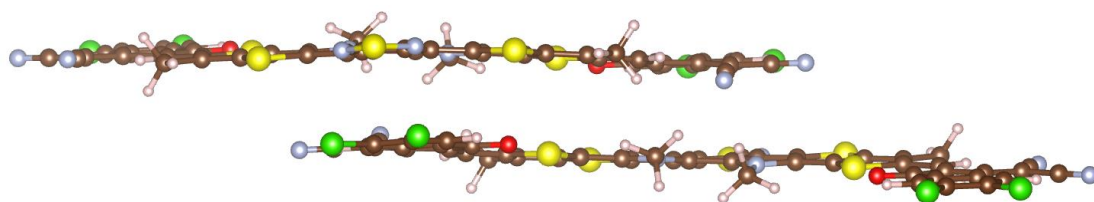

W

Figure S4. The planar and vertical feature of DBE adsorb on the BTP-eC9 dimer with W configuration. The calculated adsorption energy is -1.05 eV.

Figure S5. The calculated distance between BTP-eC9 and BTP-eC9, which is 4.4Å.
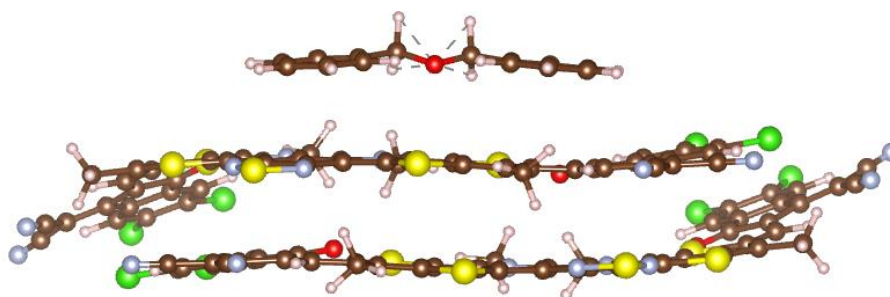
Figure S6. The calculated distance between BTP-eC9 and BTP-eC9 after the DBE adsorption, which is 2.9 Å.
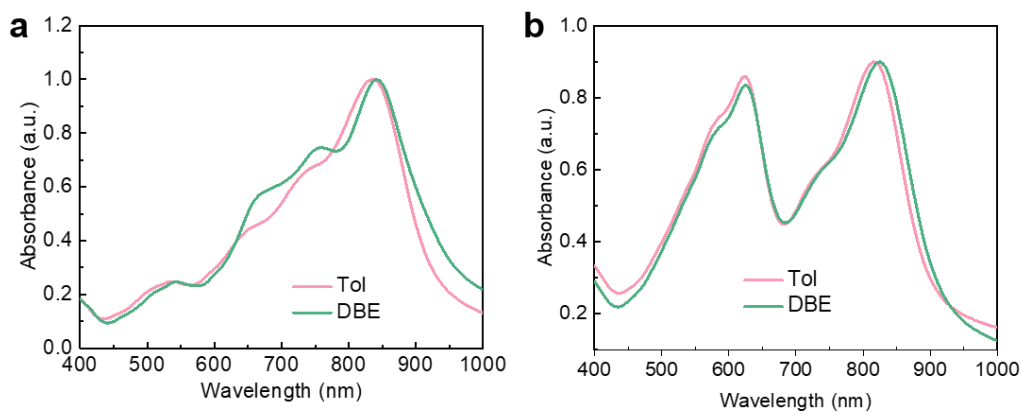
Figure S7. The absorption curves of BTP-eC9 without and with DBE additive.

Table S1. The IP and OOP parameter of BTP-eC9 without and with ether additive.

	BTP-eC9 (Tol)	BTP-eC9 (DBE)
OOP π location	1.69 Å^{-1}	polycrystalline
d-spacing	3.72 Å	polycrystalline
CCL	21.6 Å	polycrystalline
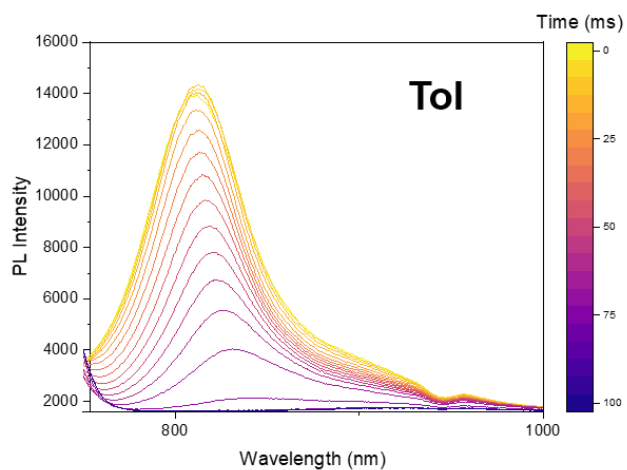
Figure S8. The PL curves as a function of spin time for PM6:BTP-eC9 film casted by neat toluene solvent.
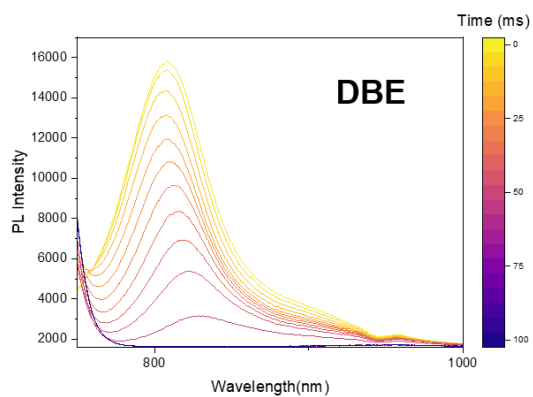
Figure S9. The PL curves as a function of spin time for PM6:BTP-eC9 film casted with DBE additive incorporation.
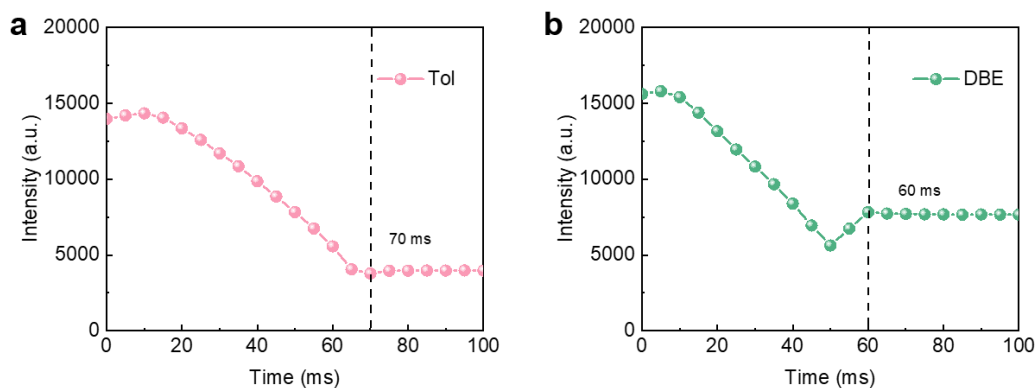
Figure S10. The evolution of the in-situ PL intensity (at 700 nm) of PM6:BTP-eC9 blend without and with ether additive.
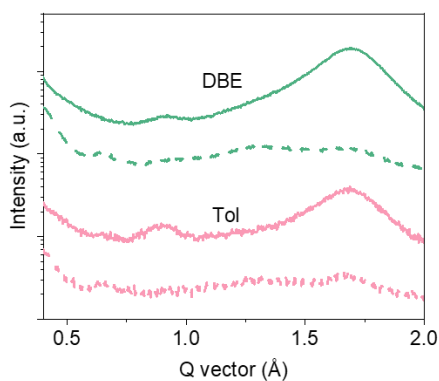
Figure S11. The In-plane and out-of-plane profiles of the corresponding 2D GIWAXS patterns. The pink curve is extracted from GIWAXS profile of blend film casted by neat toluene solvent. The green curve is extracted from the GIWAXS profile of blend film casted by toluene solvent with DBE additive. The solid line represents the out-of-plane direction. The dash line represents the in-plane direction.

Table S2. The IP and OOP parameter of PM6:BTP-eC9 without and with ether additive.

	Tol	DBE
OOP peak location	1.69 Å^{-1}	1.69 Å^{-1}
d-spacing	3.72 Å	3.71 Å
CCL	21.2 Å	25.5 Å
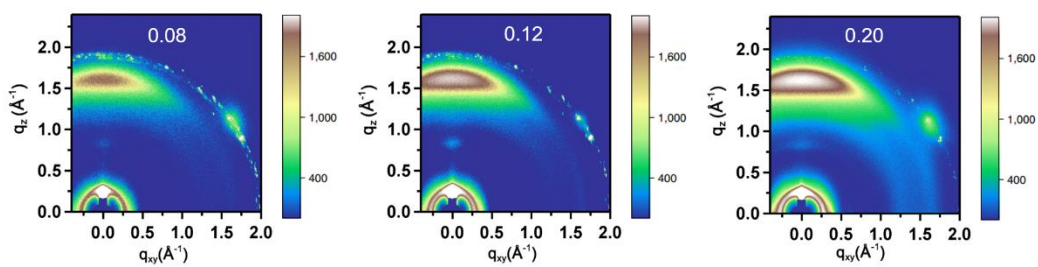
Figure S12. The 2D GIWAXS patterns of toluene-casted PM6:BTP-eC9 blend film with varied incident angle.
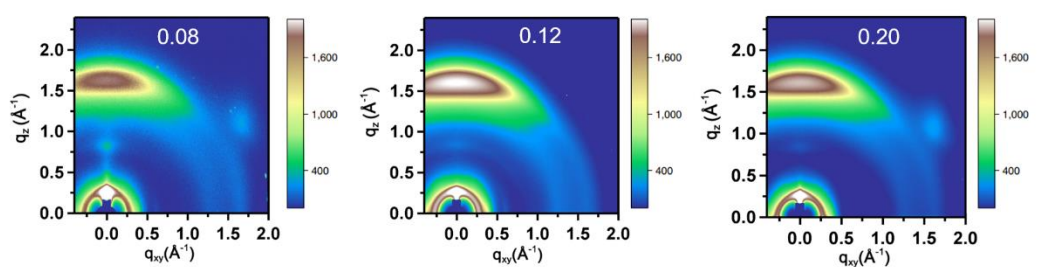
Figure S13. The 2D GIWAXS patterns of toluene-casted PM6:BTP-eC9 blend film with the DBE additive incorporation with the varied incident angle.
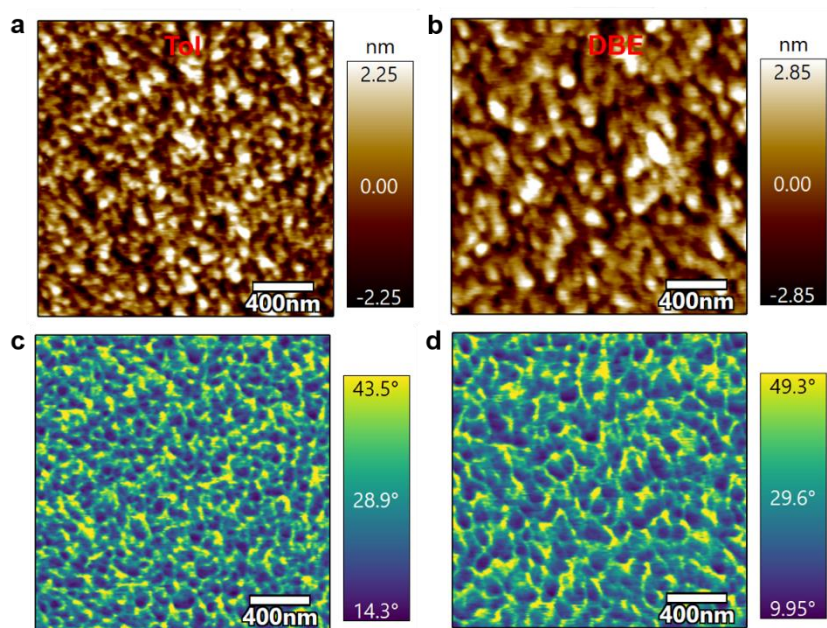

Figure S14. The topography of PM6:BTP-eC9 by toluene (a) and DBE addition (b); The phase image of PM6:BTP-eC9 by toluene (c) and DBE addition (d).

Measurement Report

Report No. 24TR052304

Client Name	Changzhou University
Client Address	No. 21 Gehu Road, Wujin District, Changzhou, Jiangsu, China
Sample	Organic solar cell
Manufacturer	Changzhou University
Measurement Date	23th May, 2024

Performed by:	Qiang Shi *Qiang Shi*	Date: 23/05/2024
Reviewed by:	Wenjie Zhao *Wenjie Zhao*	Date: 23/05/2024
Approved by:	Yucheng Liu *Yucheng Liu*	Date: 23/05/2024

Sample Information

Sample Type	Organic solar cell
Serial No.	28-1-2
Lab Internal No.	24052301-4#
Measurement Item	I-V characteristic
Measurement Environment	24.2±2.0°C,41.7±5.0%R.H

Measurement of I-V characteristic

Reference cell	PVM1121
Reference cell Type	mono-Si, WPVS, calibrated by NREL (Certificate No. ISO 2098)
Calibration Value/Date of Calibration for Reference cell	143.95mA/ Feb. 2024
Measurement Conditions	Standard Test Condition (STC): Spectral Distribution: AM1.5 according to IEC 60904-3 Ed.3, Irradiance: 1000±50W/m², Temperature: 25±2°C
Measurement Equipment/ Date of Calibration	AAA Steady State Solar Simulator (YSS-T155-2M) / July.2023 IV test system (ADCMT 6246) / June. 2023 Measuring Microscope (MF-B2017C) / July.2023
Measurement Method	I-V Measurement: Dual-lamp solar simulator spectral distribution adjusted to make the match factor within 1.00±0.02, Irradiance adjusted to 1 Sun according to reference cell calibration value. Logarithmic sweep in both directions (Voc to Isc and Isc to Voc) during one flash based on IEC 60904-1:2020;
Measurement Uncertainty	Isc: 2.0%(k=2); Voc: 1.0%(k=2); Pmax: 2.4%(k=2)

====**Measurement Results** ====

	Forward Scan (Isc to Voc)		Reverse Scan (Voc to Isc)	
Area		3.80 mm²		
Isc	1.058	mA	1.058	mA
Voc	0.870	V	0.870	V
Pmax	0.718	mW	0.719	mW
Ipm	0.971	mA	0.972	mA
Vpm	0.739	V	0.740	V
FF	78.02	%	78.12	%
Eff	18.90	%	18.92	%

- Area was provided by the client.
- Test results listed in this measurement report refer exclusively to the mentioned measured sample.
- The results apply only at the time of the test, and do not imply future performance.

DUT_Lab_SN: 24052301-4#

– – – Voc to Isc
——— Isc to Voc
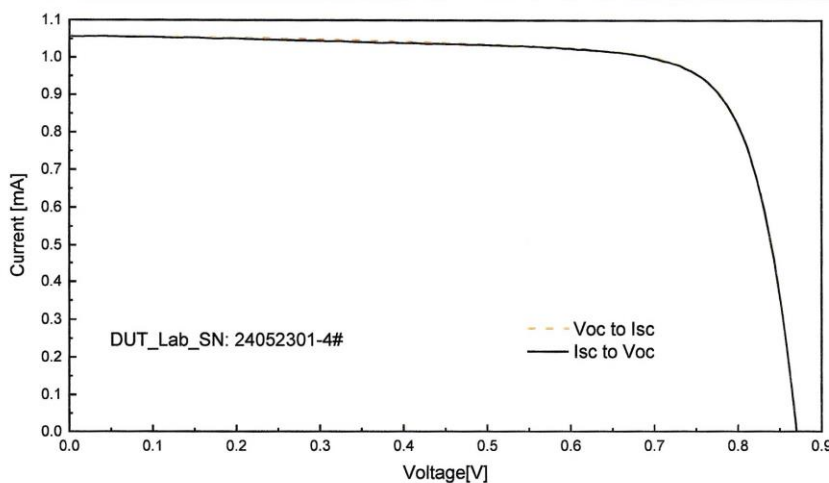
Fig.1 I-V curves of the measured sample

-------**End of Report**-------

Figure S15. Independent efficiency certification of small-area perovskite solar cells by an accredited institute of Shanghai Institute of Microsystem and Information Technology, Chinese Academy of Sciences (SIMIT), achieving a PCE of 18.9%. This report is reproduced with the permission from SIMIT.

Table S3. The photovoltaic parameters of PM6:BTP-eC9 with varied amount of DBE additive.

Process	V_{OC} (V)	J_{SC} (mA cm^{-2})	FF (%)	PCE (%)	Ave. PCE (%)[a]
Tol	0.87	25.7	76.7	17.1	16.7
0.5% DBE	0.86	28.0	80.5	19.4	19.0
1% DBE	0.85	27.1	78.2	18.0	17.5
2% DBE	0.84	24.9	74.6	15.6	15.0

a: The average PCE from 10 separate devices.

Table S4. The photovoltaic parameters of thickness-dependent toluene-casted PM6:BTP-eC9.

Thickness	V_{OC} (V)	J_{SC} (mA cm^{-2})	FF (%)	PCE (%)	Ave. PCE (%)[a]
100 nm	0.87	25.7	76.7	17.1	16.7
200 nm	0.86	26.3	71.0	16.1	15.5
300 nm	0.85	26.9	65.3	14.9	14.3

a: The average PCE from 10 separate devices.

Table S5. The photovoltaic parameters of thickness-dependent toluene-casted PM6:BTP-eC9 with DBE addition.

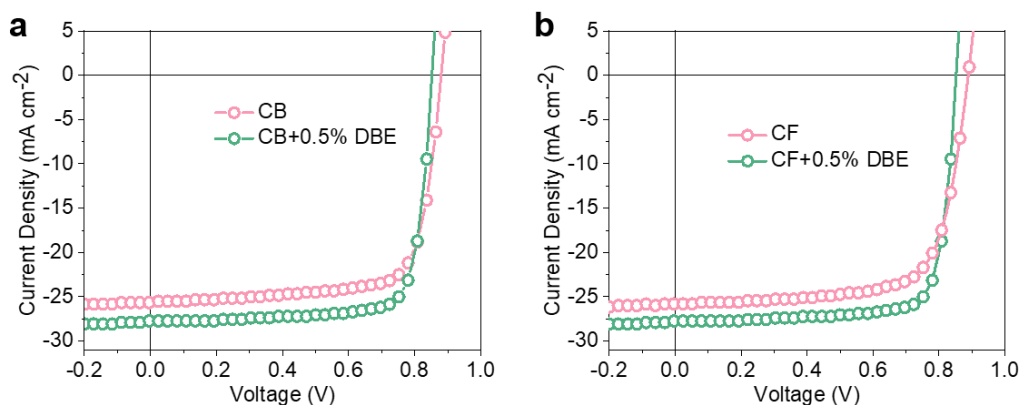| Thickness	V_{OC} (V)	J_{SC} (mA cm^{-2})	FF (%)	PCE (%)	Ave. PCE (%)[a]
100 nm	0.86	28.0	80.5	19.4	19.0
200 nm	0.86	28.0	76.1	18.3	17.9
300 nm	0.85	28.4	72.3	17.4	17.0

a: The average PCE from 10 separate devices.

Figure S16. The *J-V* curves of PM6:BTP-eC9 without and with DBE additive incorporation based on chloroform (CF) and chlorobenzene (CB) solvent.

Table S6. The photovoltaic parameter of PM6:BTP-eC9 without and with DBE additive based on CF solvent

Solvent	V_{OC} (V)	J_{SC} (mA cm^{-2})	FF (%)	PCE (%)	Ave. PCE (%)[a]
CF	0.89	26.1	71.6	16.6	16.2
DBE	0.86	27.8	77.6	18.6	18.2

a: The average PCE is from 10 separated devices.

Table S7. The photovoltaic parameter of PM6:BTP-eC9 without and with DBE additive based on CB solvent

Solvent	V_{OC} (V)	J_{SC} (mA cm^{-2})	FF (%)	PCE (%)	Ave. PCE (%)[a]
CB	0.88	25.6	74.5	17.1	16.8
DBE	0.85	27.8	79.3	18.8	18.5

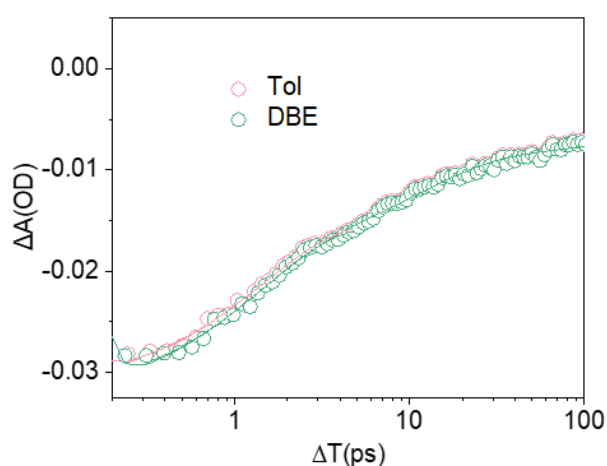a: The average PCE is from 10 separated devices.

Figure S17. The GSB dynamics probed at 590 nm of the PM6:BTP-eC9 blend films without and with DBE additive.
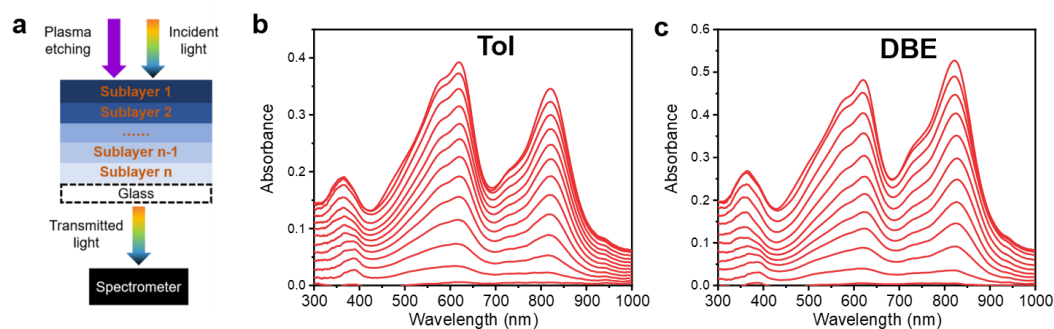
Figure S18. (a) The etching diagram of FLAS characterization. The absorption spectrum of PM6:BTP-eC9 by neat toluene (b) and DBE addition (c) by FLAS method.
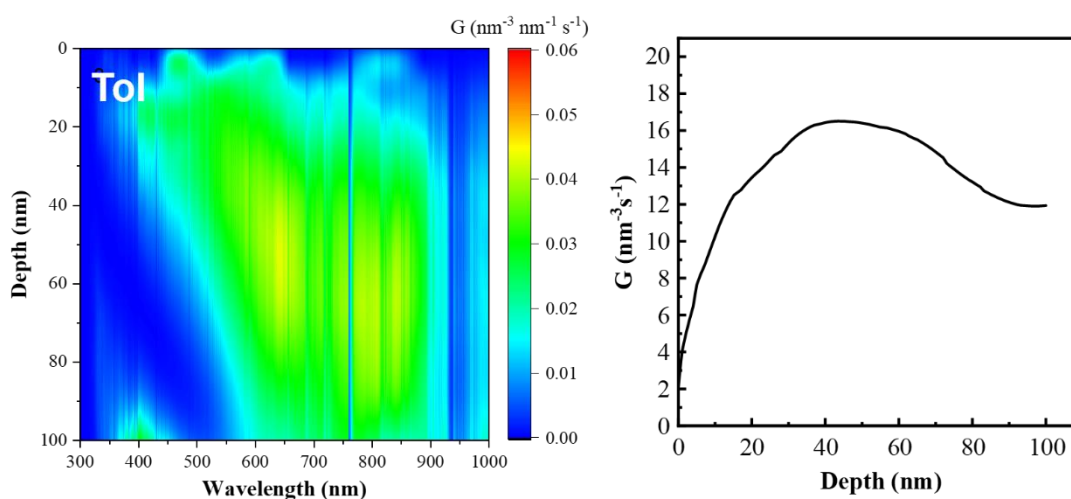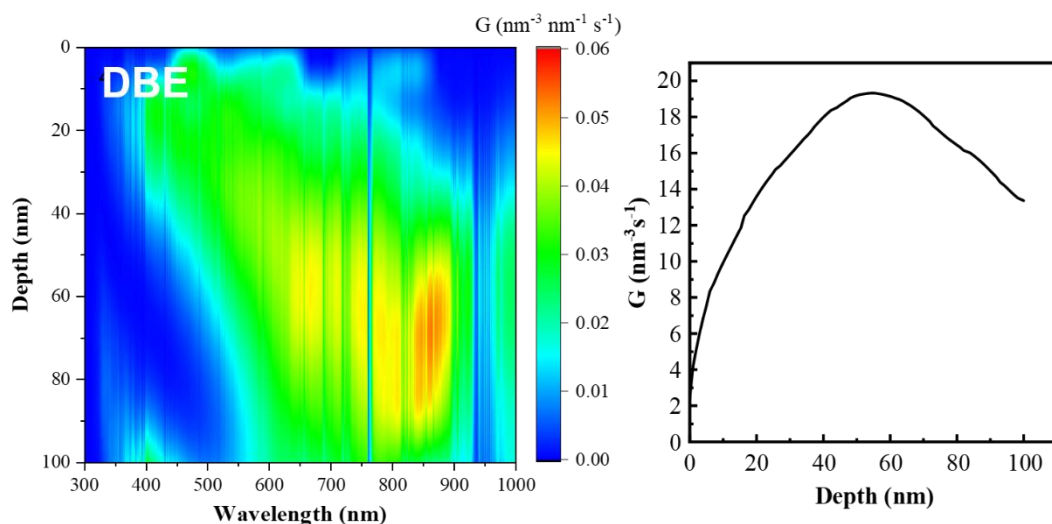

Figure S19. Film-depth-dependent light absorption spectroscopy characterizations. Numerical simulations for the exciton generation contours of toluene-casted PM6:BTP-eC9 film, where the noise arise from the fluctuation of the AM 1.5 G solar spectrum. Dependence of the simulated exciton generation rate (G) on the film depth of toluene-casted PM6:BTP-eC9 film.

Figure S20. Film-depth-dependent light absorption spectroscopy characterizations. Numerical simulations for the exciton generation contours of toluene-casted PM6:BTP-eC9 film with DBE additive, where the noise arise from the fluctuation of the AM 1.5 G solar spectrum. Dependence of the simulated exciton generation rate (G) on the film depth of toluene-casted PM6:BTP-eC9 film with DBE additive.
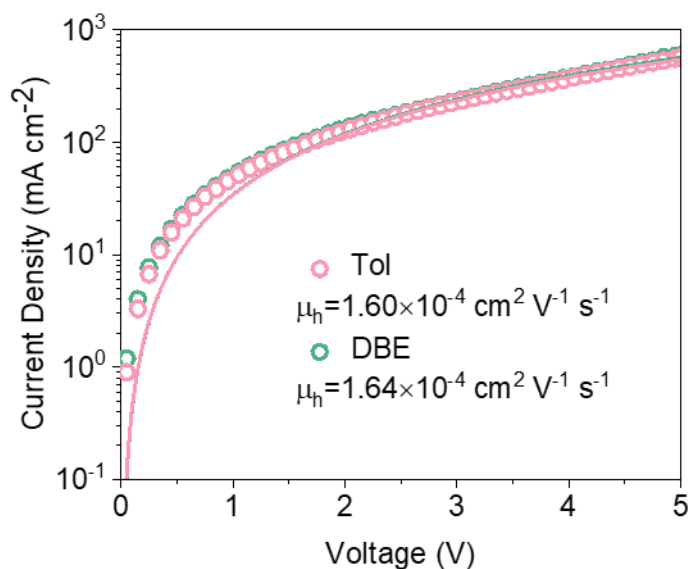

Figure S21. The dark current density-voltage curves of hole-only device for toluene-casted PM6:BTP-eC9 film without and with DBE additives.
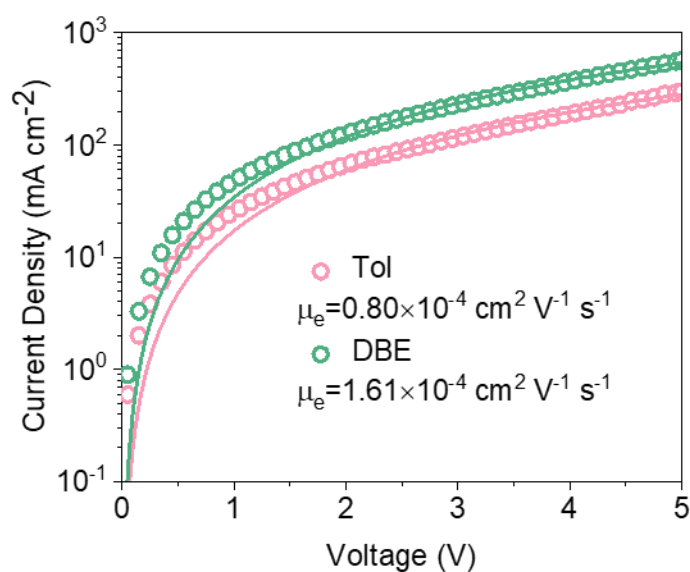
Figure S22. The dark current density-voltage curves of electron-only device for toluene-casted PM6:BTP-eC9 film without and with DBE additives.
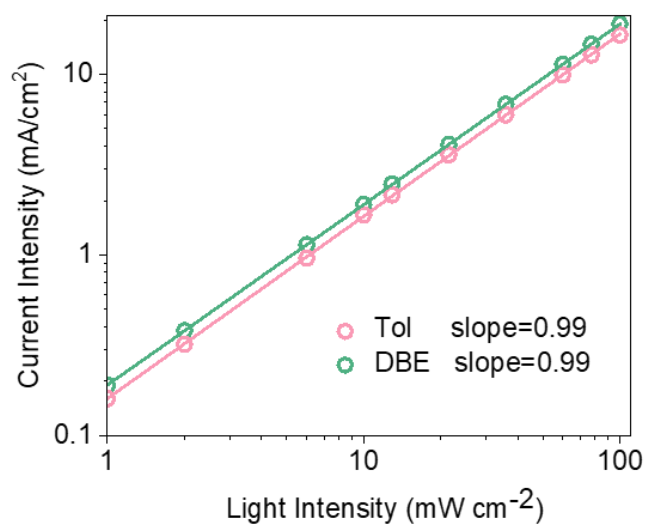

Figure S23. The current density-light intensity curves of toluene-casted PM6:BTP-eC9 device without and with DBE additives.
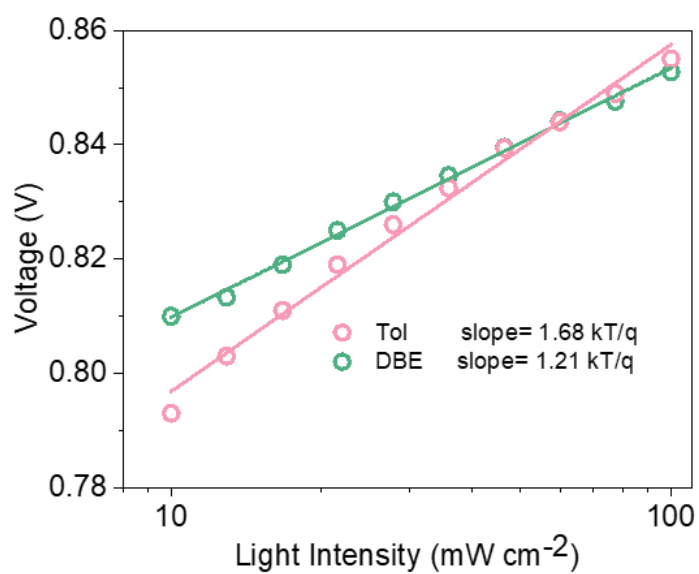
Figure S24. The voltage-light intensity curves of toluene-casted PM6:BTP-eC9 device without and with DBE additives.
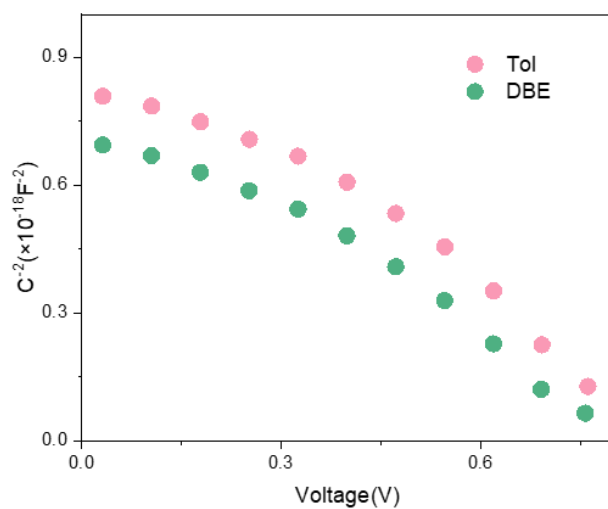

Figure S25. The capacitance-voltage curves for toluene-casted PM6:BTP-eC9 device without and with ether additive.
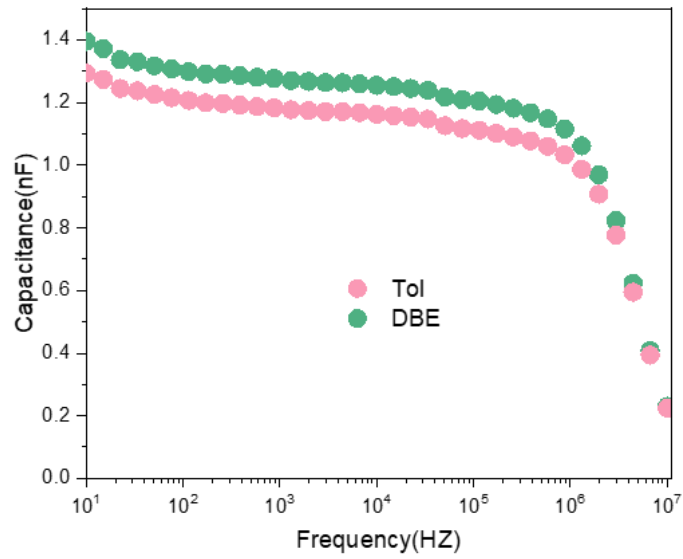
Figure S26. The capacitance-frequency curves for toluene-casted PM6:BTP-eC9 device without and with ether additive.
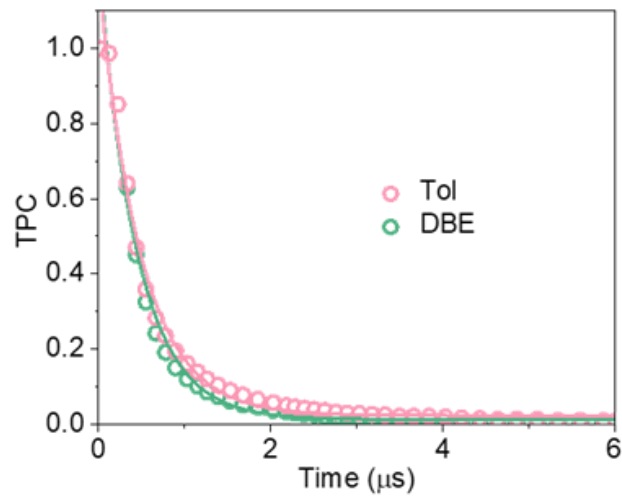

Figure S27. The TPC curves of toluene-casted PM6:BTP-eC9 device without and with DBE additives.

Reference

1. Kresse, G.; Furthmüller, J., Efficient iterative schemes for ab initio total-energy calculations using a plane-wave basis set. Physical Revivew B **1996,** 54, 16, 11169.

2. Christoph Bannwarth, Sebastian Ehlert, Stefan Grimme et al.,GFN2-xTB—An Accurate and Broadly Parametrized Self-Consistent Tight-Binding Quantum Chemical Method with Multipole Electrostatics and Density-Dependent Dispersion Contributions. Journal of Chemistry Theory Computation **2019**, 15, 3, 1652–1671.

3. Guanyu Lu, Zichao Shen, Hong Wang, Laju Bu, and Guanghao Lu, Optical interference on the measurement of film-depth-dependent light absorption spectroscopy and a correction approach, Review of Scientific Instruments, 2023, 94, 023907.